Langmuir

Article

pubs.acs.org/Langmuir

Humidity Effects on the Wetting Characteristics of Poly(*N*-isopropylacrylamide) during a Lower Critical Solution Transition

Arnav Chhabra,[†,‡] Ravitej R. Kanapuram,[†,‡] Tae Jin Kim,[‡] Jianxin Geng,[§,∥] Alexandre K. da Silva,[‡] Christopher W. Bielawski,[§] and Carlos H. Hidrovo*[,‡]

[‡]Department of Mechanical Engineering, The University of Texas at Austin, 204 East Dean Keeton Street, Austin, Texas 78712, United States

[§]Department of Chemistry and Biochemistry, The University of Texas at Austin, 1 University Station, A1590, Austin, Texas 78712, United States

[∥]Technical Institute of Physics and Chemistry, Chinese Academy of Sciences, 29 Zhongguancun East Road, Haidian District, Beijing 100190, People's Republic of China

Supporting Information

ABSTRACT: Poly(*N*-isopropylacrylamide) (PNIPAM) is expected to find utility in tissue engineering and drug delivery, among other biomedical applications. These applications capitalize on the intrinsic lower critical solution temperature (LCST) of the polymer: below the LCST, enthalpic gain from intermolecular hydrogen bonding between PNIPAM and water molecules dominates the solvation; above the LCST, entropic effects resulting from the intramolecular hydrogen bonding between the carboxyl and amide groups of PNIPAM lead to water expulsion. The dependence of the LCST upon the molecular weight, solvent, and solution activity (i.e., solute concentration) has been studied extensively. However, what has not been previously explored is the effect of humidity on the characteristic properties of the polymer. Herein, we show that the relative humidity affects the water adsorption dynamics of PNIPAM as well as the magnitude of the transition that occurs at the LCST of the polymer. In short, the magnitude of the LCST transition decreases with an increasing relative humidity, and the time period over which adsorption occurs decreases with the temperature.

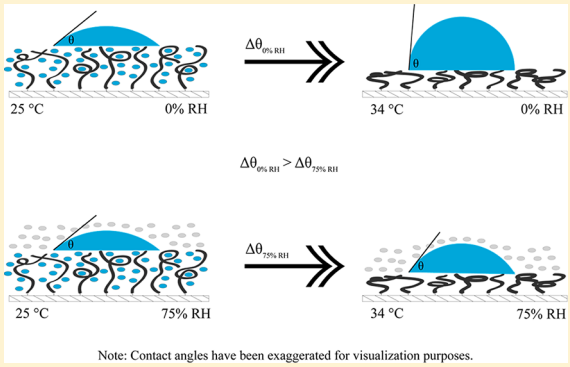

INTRODUCTION

Poly(*N*-isopropylacrylamide) (PNIPAM) has found utility in biomedical applications that require either a morphological or a surface energy change in response to changes in its environment. The property that makes PNIPAM so attractive, however,[1] is its sharp lower critical solution transition that occurs around 32 °C in aqueous solutions, above which the polymer dehydrates and precipitates.[2] Consequently, a hydrogel created from PNIPAM swells below the transition temperature and collapses above it[3] (Figure 1).

For PNIPAM, the transition temperature corresponds to the lower critical solution temperature (LCST) of the linear polymer and the volume phase transition temperature (VPTT) of the cross-linked hydrogel.[4] In addition to temperature, PNIPAM hydrogels can be made sensitive to stimuli, such as pH,[5] glucose,[6] light,[7] metal cations,[8] and many others, through clever polymer design techniques. Owing to these unique properties and its excellent biocompatibility *in vitro*,[9] PNIPAM has been extensively used in biomedical applications. Some applications that have already been explored include injectable tissue engineering scaffolds, where the loosely cross-linked PNIPAM and P(NIPAAm-*co*-AAc) are pliable at room temperature (RT) and rigid at body temperature (BT),[10] biosensors for detection of DNA,[11] drug carrier micelles, where PNIPAM segments are incorporated in either hydrophilic shells or hydrophobic cores,[12,13] and nanoscale actuation by combining PNIPAM brushes with gold nanoparticles.[14]

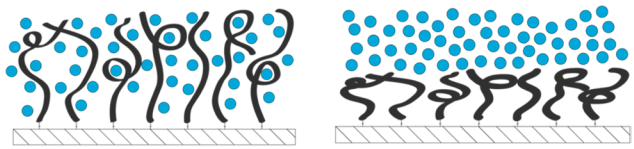

Figure 1. (a) PNIPAM hydrogel below the transition temperature where the swelled morphology occurs. (b) PNIPAM hydrogel above the transition temperature where the collapsed morphology occurs.

Received: March 21, 2013
Revised: May 14, 2013
Published: May 23, 2013

   dx.doi.org/10.1021/la401072d | *Langmuir* 2013, 29, 8116−8124

PNIPAM-modified surfaces have also been used for wettability control by reversibly switching between superhydrophobicity and superhydrophilicity.[15] Superhydrophobicity is a highly sought property because it is relevant to many areas of technology: self-cleaning surfaces,[16] drag reduction,[17−19] and waterproofing textiles.[20,21] Additionally, it should be noted that the transition temperature of PNIPAM can be modulated through co-polymerization with hydrophobic or hydrophilic monomers, thus allowing for accentuation of properties suited for the application under consideration.[22]

The objective of this work is 2-fold: (a) to understand water droplet dynamics on PNIPAM and, consequently, deduce parameters relevant to adsorption on the polymer and (b) to characterize the change in surface energy of PNIPAM in response to changes in the relative humidity. To understand the characteristics of PNIPAM, water droplets were dispensed on PNIPAM films using a syringe and imaged using a goniometer. Through image processing techniques, the contact angle of the droplet on the surface, which is a good indicator of surface energy, was ascertained for different ambient relative humidities. Furthermore, changes in the profile of a given droplet were quantified with respect to time. An increased knowledge regarding the response of PNIPAM to various thermodynamic conditions may facilitate the utility of this polymer in a broader range of biomedical applications.

BACKGROUND

LCST. The presence of a LCST for aqueous solutions of PNIPAM was first demonstrated in a seminal paper by Heskins et al.[2] To understand the process of phase separation of PNIPAM from water above the LCST, it is necessary to consider the system with a free energy perspective. The Gibbs free energy (G) is defined as

$$G \equiv H - TS \tag{1}$$

Furthermore, differentiating both sides and assuming a constant temperature yields

$$\mathrm{d}G = \mathrm{d}H - T\mathrm{d}S \rightarrow \Delta G = \Delta H - T\Delta S \tag{2}$$

For mixing to be spontaneous, the change in the Gibbs free energy induced via mixing of PNIPAM and water, ΔG_{mix}, must be less than 0. As shown by Heskins et al.,[2] the enthalpy change of the polymer−water solution ($\Delta H_{mix,solution}$) is more negative above the LCST than the enthalpy change of the separated PNIPAM and water phase ($\Delta H_{mix,biphasic}$) and, hence, more favorable. However, for temperatures above the LCST, $\Delta S_{mix,solution}$ turns out to be much smaller than $\Delta S_{mix,biphasic}$. Because of Gibbs free energy dependence upon both the enthalpic and entropic terms (eq 2), $\Delta G_{mix,biphasic}$ is lower than $\Delta G_{mix,solution}$ up to a certain mole fraction of the polymer and, thus, more favorable. Physically, this refers to the domination of entropic effects (expression of hydrophobic portions resulting in expulsion of water from the polymer matrix) over the enthalpic effects (formation of hydrogen bonds between the polymer and water) at temperatures above the LCST.[23]

The LCST for linear PNIPAM also corresponds to the VPTT of the hydrogel. The cross-linked hydrogel particles exhibit a significant decrease in the particle size above the VPTT, and the hydrogel subsequently collapses.[24,25] During this transition, the hydrogel rejects water from its pore and increases its stiffness and opacity.[24,26] This transition happens to be reversible, allowing for the cross-linked hydrogel to swell again as the temperature is decreased below the VPTT. However, this reswelling process turns out to be slower than the shrinking process that precedes it.[26]

Evaporation Models. Two extreme models of droplet evaporation can be categorized as pinned (varying contact angle and constant wetting distance) or unpinned (constant contact angle and varying wetting distance)[27,28] (Figure 2).

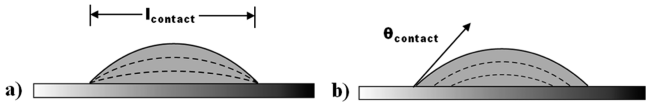

Figure 2. (a) Dynamic pinned evaporation model. As the droplet evaporates, its edge remains affixed to the sample and the length of the contact line ($l_{contact}$) remains constant. (b) Dynamic unpinned evaporation model. As the droplet evaporates, the contact angle ($\theta_{contact}$) remains constant and the edge of the droplet recedes inward.

For the dynamic unpinned model (Figure 2b), experiments have shown that $\bar{V}^{2/3}$ decreases linearly with time, where $\bar{V}$ is the volume of the droplet.[29] Unfortunately, to the authors' knowledge, an analytical model does not exist for the pinned case. To characterize the change in volume for the pinned case, it is necessary to understand that the motive force for evaporation is the difference in the water vapor concentration between the surface of the droplet and the air surrounding it. On the basis of the diffusion equation, Picknett et al. were able to deduce the rate of change of the droplet volume in the pinned scenario.[29]

$$\frac{\mathrm{d}\bar{V}}{\mathrm{d}t} = -2\pi D\Delta P\frac{M}{\rho RT}f\left(\frac{3\bar{V}}{\pi\beta}\right)^{1/3} \tag{3}$$

In eq 3, $\bar{V}$ is the volume of the droplet, D is the diffusion coefficient of vapor molecules occupying the surrounding air, ΔP is the difference between the saturation vapor pressure of the liquid at the prescribed temperature (P_o) and the partial pressure of the vapor far from the surface of the droplet (P_∞), M is the molar mass, ρ is the density of the liquid, R is the gas constant, T is the absolute temperature, $\beta = (1 - \cos(\theta))^2(2 + \cos(\theta))$, and f is an empirical function based on θ. The approximate correlations for f can be found in the paper by Picknett et al.[29] On the basis of certain approximations and rearrangements, Schönfeld et al.[27] were able to derive a function for the volume of the pinned droplet with respect to time.

$$\bar{V}(t) = \bar{V}_o - 2\pi D\Delta P\frac{\alpha M}{\rho RT}\frac{f(\theta_o/\alpha)}{\sin(\theta_o/\alpha)}t \rightarrow \bar{V}(t) \propto t \tag{4}$$

where θ_o is the contact angle of the droplet at time $t = 0$ and α is a dimensionless correction factor. Equation 4 suggests that, for pinned evaporation, volume decays linearly with time.

Water Adsorption on PNIPAM. Because PNIPAM is widely used in biomedical applications, water uptake by the polymer can have dire consequences on the system. The uptake can lead to physiochemical changes in the polymer, which can cause problems, such as reduced adhesion, amplified chemical aging, swelling/expansion, and diminished biocompatibility.[30−34] Because of these reasons, it is important to understand and characterize the water uptake by PNIPAM. Previous work assessed the efficacy of a non-contact measurement technique using fluorescence emission of 3-hydroxyflavone probes to quantify the water uptake in PNIPAM thin films.[23] The results from these studies indicate that water adsorption on PNIPAM

dx.doi.org/10.1021/la401072d | Langmuir 2013, 29, 8116−8124

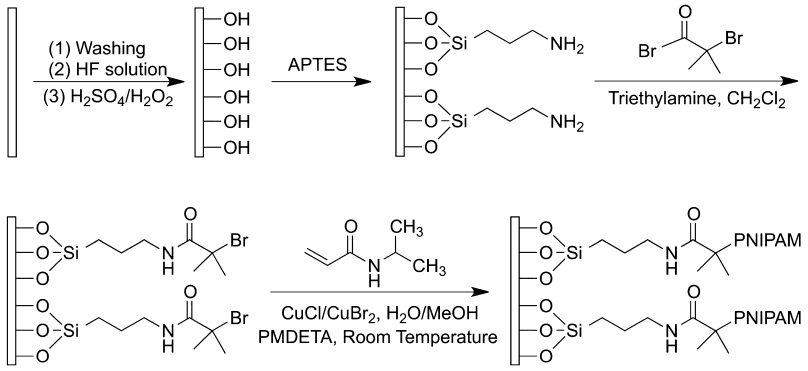

Figure 3. Graphical depiction of the surface-initiated ATRP.

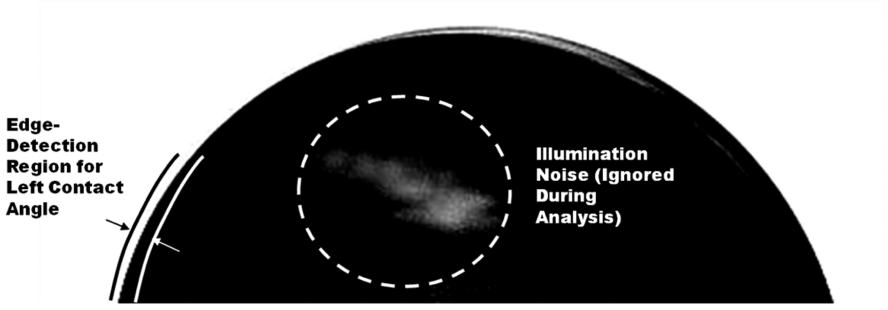

Figure 4. Sample goniometer-generated profile of a water droplet dispensed on a surface. Edge markers on the region in the left are sampled (25% of the number of sampled points in the entire droplet) and used for generating a Cartesian circular curve fit. On the basis of this curve-fit equation, a contact angle is ascertained from the local derivative. The noise generated from back illumination is ignored during the data analysis and does not affect the contact angles. A similar procedure is followed for the right-side contact angle as well.

films follows a two-phase process: (a) at low humidity, the adsorption leads to disruption in polymer−fluorophore bonding, and (b) at larger relative humidities, the relevant intensities change significantly, pointing to a dramatic change in local polarity.[23] However, to the authors' knowledge, no previous work has attempted to characterize the water uptake of PNIPAM, especially under different ambient temperatures and relative humidities. With full characterization of adsorption on PNIPAM, it would be easier for researchers to predict which thermodynamic conditions would help minimize surface physiochemical changes resulting from water uptake.

EXPERIMENTAL SETUP AND METHODOLOGY

PNIPAM brushes were synthesized using the process of atom transfer radical polymerization (ATRP), which is well-documented in the literature.[35−38] The prepared brushes were uniform in nature, and the film thickness increased with the polymerization time, as seen from the atomic force microscopy (AFM) characterization images presented in Figures S2−S4 of the Supporting Information.

Silicon Wafer Preparation. A Si wafer with a 30 nm SiO_2 film was sonicated in 20% HF aqueous solution for 10 min. The wafer was then cleaned using acetone, ethanol, and deionized water with sonication for 5 min in succession. The wafer was then etched in 5% HF aqueous solution and treated with Piranha solution by sonication. Afterward, the wafer was rinsed with deionized water and acetone and then dried using nitrogen. The wafer was then treated with a 1.25% (3-aminopropyl)triethoxysilane (APTES) solution in toluene at 115 °C for 30 min. Finally, the wafer was removed from the solution, sonicated in toluene for 2 min, rinsed with acetone, and dried under nitrogen.

Amidation. A dry flask under nitrogen was charged with 47 mL of dry dichloromethane, 2 mL of dry triethylamine, and the aforementioned Si wafer. After cooling the reaction flask to 0 °C, 1 mL of 2-bromomethylpropionyl was added over the course of 10 min. The ice bath was removed to allow for the reaction to warm to room temperature. After 21 h, the wafer was removed from the reaction flask, rinsed with toluene and acetone, and then dried under nitrogen.

Polymerization. A 200 mL Schlenk flask was charged with CuCl/$CuBr_2$ (50:1 in mole, 18.24 mg), *N*,*N*,*N*′,*N*′,*N*″-pentamethyldiethylenetriamine (PMDETA, 0.184 mL, 0.88 mmol), *N*-isopropylacrylamide (NIPAM, 3.984 g, 35.2 mmol), MeOH/deionized water (1:1, v/v, 64 mL total). The resulting solution was then degassed by 4 freeze−thaw cycles. A separate Schlenk flask (250 mL) was charged with the amidated Si wafer and then degassed. Afterward, 36 mL of the Cu-containing solution was added to the flask containing the Si wafer. After a certain period of time, the Si was removed from the reaction vessel, sonicated in a mixture of ethanol and deionized water for 2 min, and then soaked in a mixture of ethanol and deionized water for 12 h.

The entire polymerization process is depicted in Figure 3.

Sessile Drop Goniometer. A sessile drop goniometer (Figure 4), consisting of a CMOS monochrome camera (DMK 72BUC02, The Imaging Source) and a light-emitting diode (LED) array for back illumination, was used to image droplets, and the images were decomposed for further processing with MATLAB. The contact angles were measured as a function of time and other thermodynamic parameters.

Environmental Chamber. An environmental chamber was used to provide a thermodynamically controlled environment for the sessile droplets (Figure 5). A syringe needle was attached to the top of the chamber, and a set volume of deionized water was dispensed on the sample. For temperature modulations, several cartridge heaters were placed within a finned element and were controlled in parallel via a direct current (DC) power supply (Agilent E346x) based on the temperature measurements from thermocouples installed at five different locations in the chamber. The relative humidity was maintained using two separate hydraulic lines with dry air and humidified air, and the humidity was measured with a hygrometer (Omega, CNiTH series). On the basis of proper control of the flow

dx.doi.org/10.1021/la401072d | *Langmuir* 2013, 29, 8116−8124

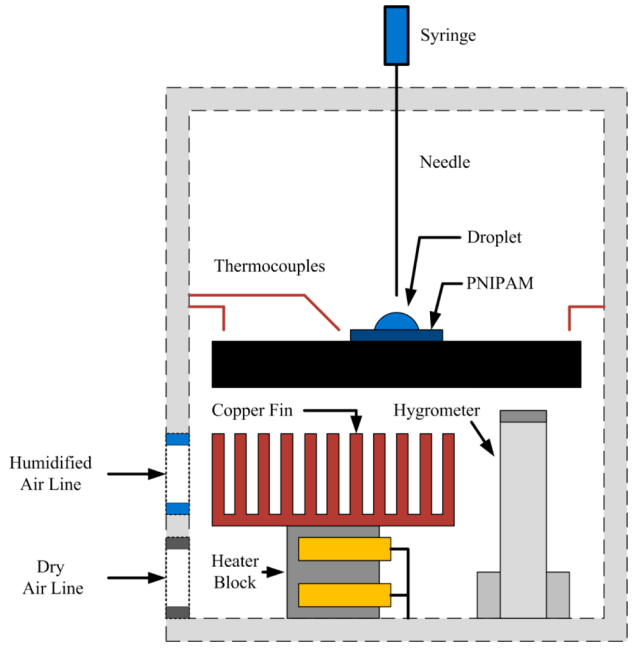

Figure 5. Cross-section of the environmental chamber depicting the following: rotary syringe needle, sample, vertically adjustable stage, finned heater, humidified and dry air lines, K-type thermocouples, and hygrometer. A thermocouple is attached close to the sample to monitor the temperature of the sample.

rate and the exposure time of the two lines, a desired global humidity was attained within the confines of the chamber.

The control structure for the environmental chamber consists of components to control both the relative humidity and temperature (Figure 6). To trace the flow of information in the control system for the environmental chamber, please refer to panels a and b of Figure S1 of the Supporting Information.

Experimental Protocol. A total of four experiments were conducted on a PNIPAM sample with a pillar height of 115 nm (~ ±3 nm). A single silicon wafer was used for the experiments; however, droplets were dispensed on different locations on the sample. Each individual experiment was performed at a constant temperature (25, 28, 31, or 34 °C), while the relative humidity was increased from 0 to 75% (0, 20, 40, 60, and 75%).

Prior to each experiment, the water in the syringe was flushed and replenished with fresh deionized water. The syringe was then securely attached to the environmental chamber and aligned to ensure that it was centered with respect to the stage. For each set point, the temperature within the environmental chamber was controlled using a proportional−integral−derivative (PID) controller and the relative humidity was set by controlling the flow rate of the dry air. Once the temperature and relative humidity were stabilized, the PNIPAM sample was removed from a sealed container filled with silica gel desiccants. The sample was then carefully rinsed with deionized water, dried with nitrogen, and placed in the environmental chamber. Control experiments were run initially to quantify the effects of cleaning on the data collected. The contact angle data acquired after the cleaning was within the uncertainty bounds of the angles calculated before the cleaning, suggesting that the cleaning process did not affect the results significantly. Additionally, there was little to no change observed in the contact angles after several cleaning cycles. The reason for placing the PNIPAM sample after the environmental chamber reached the designated set point was to replicate actual applications, where PNIPAM products were initially kept under a dry seal and then exposed to the environment.

Using a CMOS camera with an attached Nikon 200 mm macro lens for observation, the sample was placed under the syringe needle with enough space for the droplet to spread. During this process, sufficient space was provided above the sample and below the bottom of the needle for a droplet to stand unperturbed upon the sample. To allow the temperature of the sample to equilibrate with the ambient temperature, the sample was left in the chamber for 5 min before dispensing any droplets. Assuming a lumped capacitance model for the sample ($Bi \ll 0.1$), the time constant for heating/cooling was calculated to be approximately 1.25 min. A total of 5 min (four time constants) allows for the sample to reach within 98% of the set point temperature.

A droplet was then dispensed on the sample using the syringe attached to a spring loaded system. Once the droplet made contact with the sample, the syringe was retracted back to its original position. The images were acquired right before the droplet was dispensed, and 200 images (f, $^1/_{11}$; exposure time, 0.9 ms) were taken for each droplet at 5 frames per second. The sample was then repositioned to a new location, and the procedure was repeated. A total of three droplets were dispensed at each relative humidity and temperature combination, where each droplet was dispensed at a different location.

After every nine droplets, the sample was rinsed with deionized water, air-dried with nitrogen, and placed back into the environmental chamber. At the end of the experiment, the sample was cleaned in a similar fashion and placed back into the airtight-sealed container containing silica gel desiccants.

RESULTS AND DISCUSSION

Experimental Characterization of Droplet Evaporation on PNIPAM. To accurately understand the droplet dynamics on the PNIPAM samples, it is important to introduce pertinent parameters related to evaporation. Time-dependent non-dimensionalized volume and contact-line length for PNIPAM at 28 °C and 0% relative humidity are presented in Figure 7. The volume is non-dimensionalized based on the initial volume (at $t = 0$), whereas the contact-line length is non-

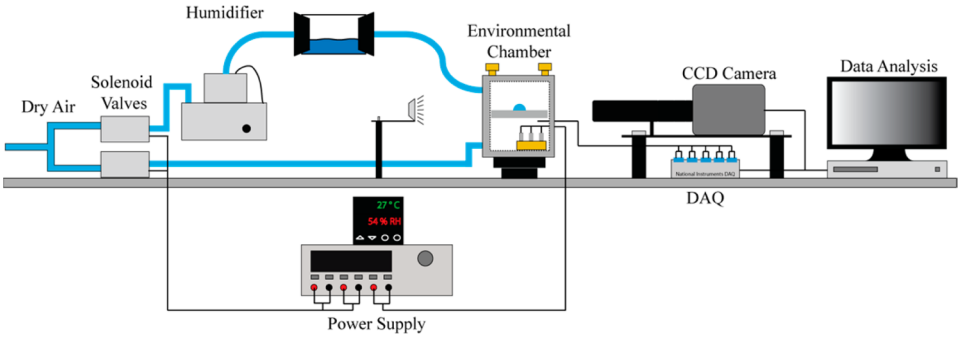

Figure 6. Surface characterization experimental setup consisting of (a) sessile drop goniometer, (b) environmental chamber, and (c) humidity/temperature control structures.

dx.doi.org/10.1021/la401072d | Langmuir 2013, 29, 8116−8124

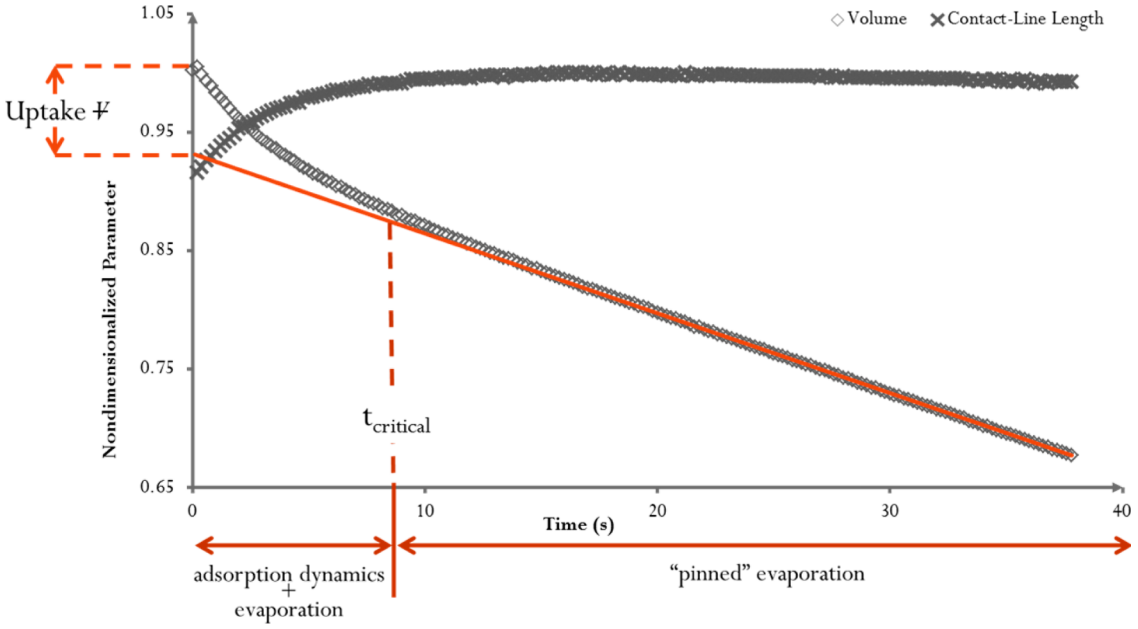

Figure 7. Non-dimensionalized volume and contact-line length of a water droplet on PNIPAM at 28 °C and 0% relative humidity. $l_{contact}$ exhibits a nonlinear increase and then a constancy region, indicating that pinned evaporation is the dominant mechanism beyond time $t_{critical}$.

dimensionalized based on the final length (as $t \rightarrow \infty$). On the basis of the data presented, two distinct trends can be observed.

The non-dimensionalized contact-line length ($l_{contact}$) increases nonlinearly up to a certain point, after which $l_{contact}$ levels off with time. Once $l_{contact}$ becomes constant, the droplet emulates a pinned evaporation model. According to Schönfeld et al., pinned evaporation is expected to follow a linear decay model[27] (eq 5).

$$\bar{V}(t) = \bar{V}_o - 2\pi D\Delta P \frac{\alpha M}{\rho RT} \frac{f(\theta_o/\alpha)}{\sin(\theta_o/\alpha)} t \rightarrow \bar{V}(t) \propto t \quad (5)$$

However, as seen in Figure 7, a nonlinear decay in volume is initially observed and is then followed by the linear volumetric decay after a certain time ($t_{critical}$). The $t_{critical}$ is defined to be the time where the second derivative of non-dimensional volume change was calculated to be zero. Because the latter phase conforms to a linear correlation between time and volumetric decay, evaporation dominates after $t_{critical}$. Before the $t_{critical}$, a nonlinear volumetric decay can be observed. This trend can be attributed to a combination of pinned evaporation and water adsorption on PNIPAM, which implies an uptake of fluid by the PNIPAM polymer. As depicted in Figure 7, if the linear trend is extrapolated back to $t = 0$, the effects of water adsorption and evaporation can be distinguished in the nonlinear region. The non-dimensionalized uptake volume can be calculated by integrating the volumetric change from $t = 0$ to $t_{critical}$, with the extrapolated line set as the baseline. The critical time can be used as a characteristic time to demarcate the water adsorption period on PNIPAM and, thus, used to characterize the time responsiveness of the polymer to external stimuli.

Dependence of the Critical Time upon the Temperature and Relative Humidity. The critical time was calculated under a varying relative humidity for each temperature set point studied. Two notable phenomena were observed during analysis of the recorded data. At a constant relative humidity, $t_{critical}$ decreases with an increasing temperature. Consequently, an increase in the temperature indicates a decrease in the amount of time that adsorption has to occur on the particular PNIPAM sample. The difference between $t_{critical}$ at the low and high temperatures was additionally noted for a series of relative humidities. The decrease in $t_{critical}$ is much higher at higher relative humidities than it is at lower relative humidities. Therefore, the adsorption period can be significantly changed by increasing the temperature under high relative humidity conditions. However, at lower humidities, the temperature increase does not significantly affect $t_{critical}$. Both of these phenomena are depicted in Figure 8.

Dependence of the LCST-Induced Contact Angle Change upon Relative Humidity. The LCST acts as a temperature switch for PNIPAM. Figure 9 displays the contact angle of water on PNIPAM as a function of the temperature for 80% relative humidity, where the sudden jump in the contact angle at the LCST is termed the LCST magnitude.

The dependence of the LCST magnitude upon the ambient relative humidity is further explored by quantifying the contact angle jump for a series of humidities. For simplicity during visualization, the contact angle jump was measured from the lower temperature (25 °C) to the higher temperature (34 °C) at each humidity level. With an increasing relative humidity, the contact angle jump appeared to decrease significantly. Between 20 and 40% relative humidity, the LCST magnitude drops from 23° to 10° (Figure 10). The numerical values of the critical times and contact angles for the various relative humidities and temperatures are presented in Table 1.

Discussion. The decrease in LCST magnitude with an increasing relative humidity is likely due to a smaller change in entropy of the polymer−water solution induced by the increasing partial pressure ($\phi = P_{wv}/P_{sat,wv}$) of the water vapor surrounding the PNIPAM thin film. This phenomenon implies that the polymer−water solution undergoes a larger entropy change at lower humidities than it does at higher humidities. On the basis of eq 2, a smaller entropy change implies a larger change in the Gibbs free energy of the biphasic phase ($\Delta G_{mix,biphasic}$). Because a larger $\Delta G_{mix,biphasic}$ represents a

dx.doi.org/10.1021/la401072d | Langmuir 2013, 29, 8116−8124

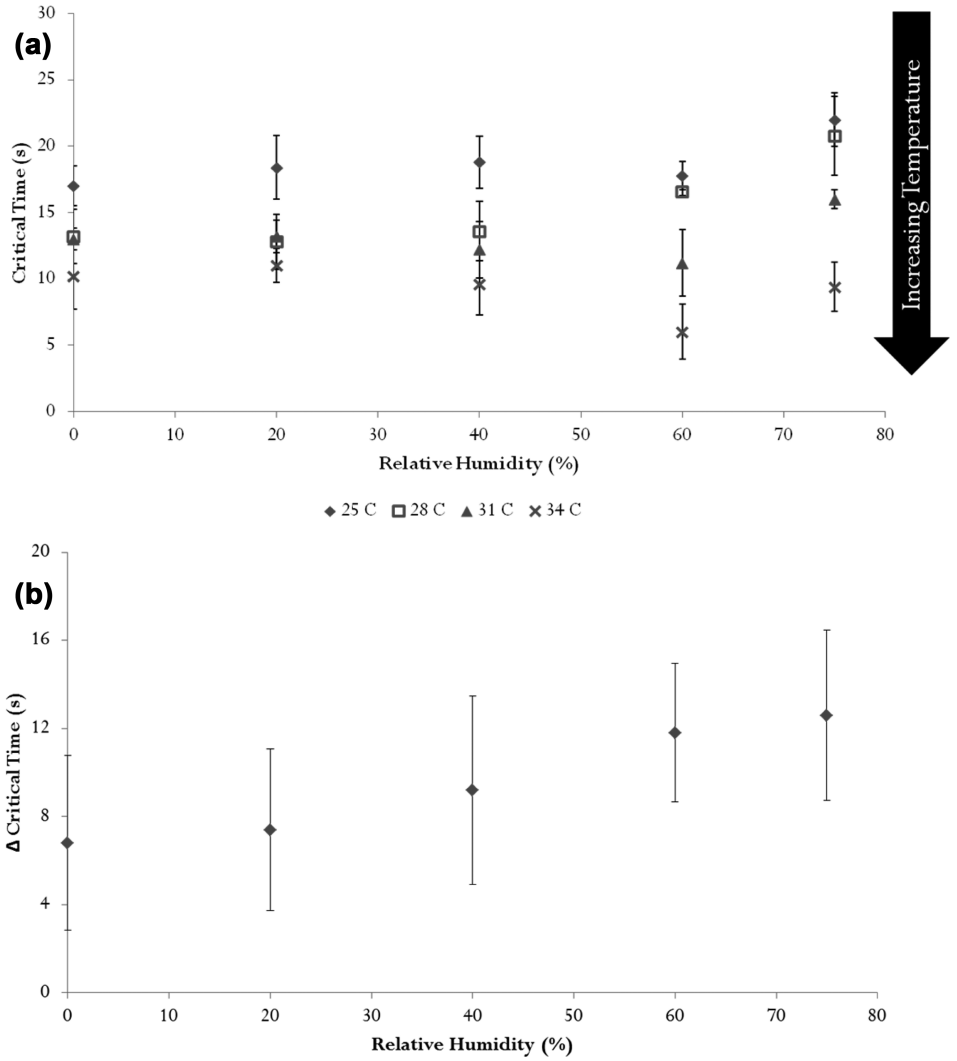

Figure 8. (a) "Critical time" ($t_{critical}$) versus relative humidity for a number of temperatures. For a given relative humidity, $t_{critical}$ decreases with an increasing temperature. The change in $t_{critical}$ between the low and high temperatures ($\Delta\ t_{critical}$), however, increases with an increasing relative humidity. (b) Change in $t_{critical}$ between the low and high temperatures ($\Delta\ t_{critical}$) versus relative humidity.

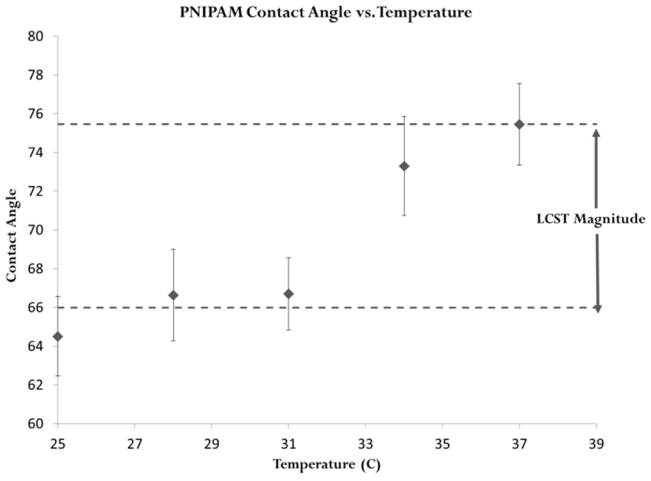

Figure 9. Static contact angle versus temperature for PNIPAM at 80% relative humidity. The LCST magnitude was found to be approximately 10°.

less favorable energy state, a higher relative humidity is expected to result in a smaller LCST magnitude.

The change in the adsorption time constant ($t_{critical}$) can be explained by the dependence of adsorption kinetics upon the partial pressure of the water vapor above the polymer and also the absolute temperature of the surroundings. The rate of adsorption, R_{ads}, can be represented as

$$R_{ads} = A\ \exp\left(-\frac{E_a}{RT}\right)(P_{wv})^x = A\ \exp\left(-\frac{E_a}{RT}\right)(\phi P_{sat,wv})^x \quad (6)$$

where A is the pre-exponential factor, E_a is the activation energy for the adsorption, R is the universal gas constant, T is the absolute temperature, ϕ is the relative humidity of the air above the polymer surface, x is the kinetic order, P_{wv} is the partial pressure of the water vapor phase above the surface, and $P_{sat,wv}$ is the saturation vapor pressure of the air and is a positive function of the absolute temperature. Equation 6 expresses the rate constant in Arrhenius form and explains the trends depicted in Figure 8. As the temperature increases, R_{ads} is expected to increase. However, the rate of adsorption (R_{ads}) is inversely proportional to the characteristic time over which adsorption occurs ($t_{critical}$). The dependence of adsorption kinetics upon relative humidity is due to the partial pressure of

dx.doi.org/10.1021/la401072d | Langmuir 2013, 29, 8116−8124

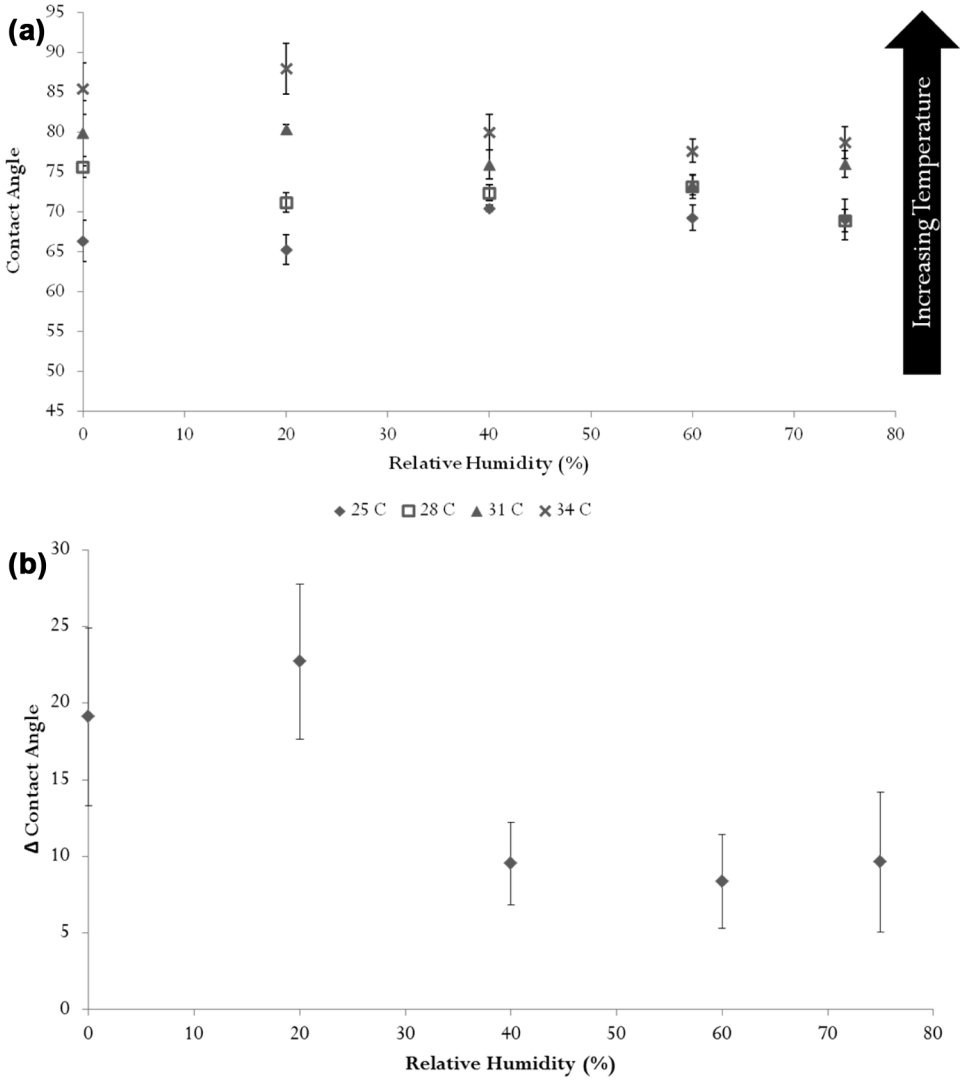

Figure 10. (a) Static contact angle of water on PNIPAM for a number of temperatures and relative humidities. (b) Contact angle difference between 25 and 34 °C at each relative humidity. The contact angle jump on PNIPAM decreases with an increasing relative humidity, with the largest decrease occurring from 20 to 40% relative humidity.

Table 1. Critical Times and Contact Angles of PNIPAM for Various Relative Humidities and Temperatures

		temperature (°C)			
	humidity (% relative humidity)	25	28	31	34
critical time (s)	0	17.00	13.20	13.00	10.20
	20	18.40	12.80	13.20	11.00
	40	18.80	13.60	12.20	9.60
	60	17.80	16.60	11.20	6.00
	75	22.00	20.80	16.00	9.40
contact angle (deg)	0	66.33	75.65	79.89	85.43
	20	65.26	71.19	80.41	87.98
	40	70.46	72.41	75.92	80.00
	60	69.31	73.16	73.37	77.66
	75	69.07	68.92	75.99	78.69

the water vapor molecules (P_{wv}) just above the polymer surface. Equation 6 suggests that R_{ads} and, thus, $t_{critical}$ are affected more by the temperature at larger relative humidities, which is in accordance with the trends displayed in Figure 8.

CONCLUSION

Herein, we examined the responsiveness of PNIPAM to changes in ambient relative humidity and studied the water uptake by the polymer. It was found that a nonlinear decrease in the volume of the droplet occurred for an initial time period (labeled $t_{critical}$), after which the volume decreased linearly. The initial change in volume was attributed to both evaporation and adsorption (water uptake by the polymer). The time-dependent diametrical profile of the droplet suggests that a "pinned" regime is the basis for evaporation on PNIPAM. Previous studies on "pinned" evaporation have shown that this regime results in a linear decrease in volume over time. On the basis of a linear extrapolation of the volume, we were able to separate the effect of evaporation from the effect of adsorption in the initial nonlinear region and further quantify the water uptake by the polymer. Our experimental results suggest that, for a given relative humidity, $t_{critical}$ decreases with an increasing temperature. However, the difference between $t_{critical}$ at low and high temperatures at a given humidity increases with an increasing relative humidity. Moreover, as the temperature of the surroundings increases above the LCST of PNIPAM or the

dx.doi.org/10.1021/la401072d | Langmuir 2013, 29, 8116−8124

VPTT of the respective hydrogel, the contact angle of water on the polymer film increases. This change in contact angle is representative of a decrease in polymer−liquid surface energy and is termed the LCST magnitude. Our results suggest that the LCST magnitude decreases with an increasing relative humidity.

■ ASSOCIATED CONTENT

Supporting Information

Flow of information in the control system of the environmental chamber used (panels a and b of Figure S1) and AFM characterization of the PNIPAM brushes (Figures S2−S4). This material is available free of charge via the Internet at http://pubs.acs.org.

■ AUTHOR INFORMATION

Corresponding Author

*E-mail: hidrovo@mail.utexas.edu.

Author Contributions

†Arnav Chhabra and Ravitej R. Kanapuram contributed equally to this work.

Notes

The authors declare no competing financial interest.

■ ACKNOWLEDGMENTS

This work was funded by The University of Texas at Austin startup funds, The University of Texas System Science and Technology Acquisition and Retention (STARS) funds, and the Norman Hackerman Advanced Research Program. Christopher W. Bielawski is grateful to the Welch Foundation (F-0046) for support. The authors of this manuscript thank Collier Miers for fabricating the environmental chamber and Juan Trejo and Harrison Leva for fine-tuning the goniometer.

■ NOMENCLATURE

PNIPAM = poly(*N*-isopropylacrylamide)
LCST = lower critical solution temperature
VPTT = volume phase transition temperature
ATRP = atom transfer radical polymerization

■ REFERENCES

(1) Pelton, R. Temperature-sensitive aqueous microgels. *Adv. Colloid Interface Sci.* **2000**, *85* (1), 1−33.

(2) Heskins, M.; Guillet, J. E. Solution properties of poly(N-isopropylacrylamide). *J. Macromol. Sci., Chem.* **1968**, *2* (8), 1441−1455.

(3) Plunkett, K. N.; Zhu, X.; Moore, J. S.; Leckband, D. E. PNIPAM chain collapse depends on the molecular weight and grafting density. *Langmuir* **2006**, *22* (9), 4259−4266.

(4) Guan, Y.; Zhang, Y. PNIPAM microgels for biomedical applications: From dispersed particles to 3D assemblies. *Soft Matter* **2011**, *7* (14), 6375−6384.

(5) Zhou, S.; Chu, B. Synthesis and volume phase transition of poly(methacrylic acid-*co*-*N*-isopropylacrylamide) microgel particles in water. *J. Phys. Chem. B* **1998**, *102* (8), 1364−1371.

(6) Zhang, Y.; Guan, Y.; Zhou, S. Synthesis and volume phase transitions of glucose-sensitive microgels. *Biomacromolecules* **2006**, *7* (11), 3196−3201.

(7) Gorelikov, I.; Field, L. M.; Kumacheva, E. Hybrid microgels photoresponsive in the near-infrared spectral range. *J. Am. Chem. Soc.* **2004**, *126* (49), 15938−15939.

(8) Luo, Q.; Guan, Y.; Zhang, Y.; Siddiq, M. Lead-sensitive PNIPAM microgels modified with crown ether groups. *J. Polym. Sci., Part A: Polym. Chem.* **2010**, *48* (18), 4120−4127.

(9) Naha, P. C.; Bhattacharya, K.; Tenuta, T.; Dawson, K. A.; Lynch, I.; Gracia, A.; Lyng, F. M.; Byrne, H. J. Intracellular localisation, geno- and cytotoxic response of poly *N*-isopropylacrylamide (PNIPAM) nanoparticles to human keratinocyte (HaCaT) and colon cells (SW 480). *Toxicol. Lett.* **2010**, *198* (2), 134−143.

(10) Stile, R. A.; Burghardt, W. R.; Healy, K. E. Synthesis and characterization of injectable poly(*N*-isopropylacrylamide)-based hydrogels that support tissue formation in vitro. *Macromolecules* **1999**, *32* (22), 7370−7379.

(11) Ali, M. M.; Aguirre, S. D.; Xu, Y.; Filipe, C. D.; Pelton, R.; Li, Y. Detection of DNA using bioactive paper strips. *Chem. Commun. (Cambridge, U. K.)* **2009**, *43*, 6640−6642.

(12) Cammas, S.; Suzuki, K.; Sone, C.; Sakurai, Y.; Kataoka, K.; Okano, T. Thermo-responsive polymer nanoparticles with a core−shell micelle structure as site-specific drug carriers. *J. Controlled Release* **1997**, *48* (2−3), 157−164.

(13) Wei, H.; Zhang, X. Z.; Zhou, Y.; Cheng, S. X.; Zhuo, R. X. Self-assembled thermoresponsive micelles of poly(*N*-isopropylacrylamide-*b*-methyl methacrylate). *Biomaterials* **2006**, *27* (9), 2028−2034.

(14) Mitsuishi, M.; Koishikawa, Y.; Tanaka, H.; Sato, E.; Mikayama, T.; Matsui, J.; Miyashita, T. Nanoscale actuation of thermoreversible polymer brushes coupled with localized surface plasmon resonance of gold nanoparticles. *Langmuir* **2007**, *23* (14), 7472−7474.

(15) Sun, T.; Wang, G.; Feng, L.; Liu, B.; Ma, Y.; Jiang, L.; Zhu, D. Reversible switching between superhydrophilicity and superhydrophobicity. *Angew. Chem., Int. Ed.* **2004**, *43* (3), 357−360.

(16) Blossey, R. Self-cleaning surfaces—Virtual realities. *Nat. Mater.* **2003**, *2* (5), 301−306.

(17) Rothstein, J. P. Slip on superhydrophobic surfaces. *Annu. Rev. Fluid Mech.* **2010**, *42* (1), 89−109.

(18) Kim, T. J.; Kanapuram, R.; Chhabra, A.; Hidrovo, C. Thermo-wetting and friction reduction characterization of microtextured superhydrophobic surfaces. *J. Fluids Eng.* **2012**, *134* (11), 114501.

(19) Kim, T. J.; Hidrovo, C. Pressure and partial wetting effects on superhydrophobic friction reduction in microchannel flow. *Phys. Fluids* **2012**, *24* (11), 112003−112018.

(20) Baxter, S.; Cassie, A. B. D. The water repellency of fabrics and a new water repellency test. *J.Text. Inst., Trans.* **1945**, *36* (4), T67−T90.

(21) Wenzel, R. N. The evaluation of textile waterproofing agents. *Am. Dyest. Rep.* **1936**, *25*, 505−514.

(22) Feil, H.; Bae, Y. H.; Feijen, J.; Kim, S. W. Effect of comonomer hydrophilicity and ionization on the lower critical solution temperature of *N*-isopropylacrylamide copolymers. *Macromolecules* **1993**, *26* (10), 2496−2500.

(23) Morris, C.; Szczupak, B.; Klymchenko, A. S.; Ryder, A. G. Study of water adsorption in poly(*N*-isopropylacrylamide) thin films using fluorescence emission of 3-hydroxyflavone probes. *Macromolecules* **2010**, *43* (22), 9488−9494.

(24) Huffman, A. S.; Afrassiabi, A.; Dong, L. C. Thermally reversible hydrogels: II. Delivery and selective removal of substances from aqueous solutions. *J. Controlled Release* **1986**, *4* (3), 213−222.

(25) Yoshitsugu, H.; Toyoichi, T. Volume phase transition in a nonionic gel. *J. Chem. Phys.* **1984**, *81* (12), 6379−6380.

(26) Hoffman, A. S. Environmentally sensitive polymers and hydrogels-smart biomaterials. *MRS Bull.* **1991**, *16* (9), 42−46.

(27) Schönfeld, F.; Graf, K.-H.; Hardt, S.; Butt, H.-J. Evaporation dynamics of sessile liquid drops in still air with constant contact radius. *Int. J. Heat Mass Transfer* **2008**, *51* (13−14), 3696−3699.

(28) Deegan, R. D.; Bakajin, O.; Dupont, T. F.; Huber, G.; Nagel, S. R.; Witten, T. A. Capillary flow as the cause of ring stains from dried liquid drops. *Nature* **1997**, *389* (6653), 827−829.

(29) Picknett, R. G.; Bexon, R. The evaporation of sessile or pendant drops in still air. *J. Colloid Interface Sci.* **1977**, *61* (2), 336−350.

(30) Bosch, P.; Fernández, A.; Salvador, E. F.; Corrales, T.; Catalina, F.; Peinado, C. Polyurethane−acrylate based films as humidity sensors. *Polymer* **2005**, *46* (26), 12200−12209.

(31) Ellison, C. J.; Miller, K. E.; Torkelson, J. M. In situ monitoring of sorption and drying of polymer films and coatings: self-referencing,

nearly temperature-independent fluorescence sensors. *Polymer* **2004**, *45* (8), 2623−2632.
(32) Goodelle, J. P.; Pearson, R. A.; Santore, M. M. Water-uptake kinetics in poly(methyl methacrylate) films with a fluorescent rotor probe. *J. Appl. Polym. Sci.* **2002**, *86* (10), 2463−2471.
(33) Olmos, D.; López-Morón, R.; González-Benito, J. The nature of the glass fibre surface and its effect in the water absorption of glass fibre/epoxy composites. The use of fluorescence to obtain information at the interface. *Compos. Sci. Technol.* **2006**, *66* (15), 2758−2768.
(34) van der Wel, G. K.; Adan, O. C. G. Moisture in organic coatings—A review. *Prog. Org. Coat.* **1999**, *37* (1−2), 1−14.
(35) Pyun, J.; Kowalewski, T.; Matyjaszewski, K. Synthesis of polymer brushes using atom transfer radical polymerization. *Macromol. Rapid Commun.* **2003**, *24* (18), 1043−1059.
(36) Edmondson, S.; Osborne, V. L.; Huck, W. T. Polymer brushes via surface-initiated polymerizations. *Chem. Soc. Rev.* **2004**, *33* (1), 14−22.
(37) Wang, J. Y.; Chen, W.; Liu, A. H.; Lu, G.; Zhang, G.; Zhang, J. H.; Yang, B. Controlled fabrication of cross-linked nanoparticles/polymer composite thin films through the combined use of surface-initiated atom transfer radical polymerization and gas/solid reaction. *J. Am. Chem. Soc.* **2002**, *124* (45), 13358−13359.
(38) Wang, S.; Zhu, Y. Facile method to prepare smooth and homogeneous polymer brush surfaces of varied brush thickness and grafting density. *Langmuir* **2009**, *25* (23), 13448−13455.